ADVANCED BIOSYSTEMS
www.adv-biosys.com

Membrane Protein Insertion into and Compatibility with Biomimetic Membranes

Tingwei Ren, Mustafa Erbakan, Yuexiao Shen, Eduardo Barbieri, Patrick Saboe, Hasin Feroz, Hengjing Yan, Samantha McCuskey, Joseph F. Hall, A. Benjamin Schantz, Guillermo C. Bazan, Peter J. Butler, Mariusz Grzelakowski, and Manish Kumar**

Membrane protein and membrane protein–mimic functionalized materials are rapidly gaining interest across a wide range of applications, including drug screening, DNA sequencing, drug delivery, sensors, water desalination, and bioelectronics. In these applications, material performance is highly dependent on activity-per-protein and protein packing density in bilayer and bilayer-like structures collectively known as biomimetic membranes. However, a clear understanding of, and accurate tools to study these properties of biomimetic membranes does not exist. This paper presents methods to evaluate membrane protein compatibility with biomimetic membrane materials. The methods utilized provide average single protein activity, and for the first time, provide experimentally quantifiable measures of the chemical and physical compatibility between proteins (and their mimics) and membrane materials. Water transport proteins, rhodopsins, and artificial water channels are reconstituted into the full range of current biomimetic membrane matrices to evaluate the proposed platform. Compatibility measurement results show that both biological and artificial water channels tested largely preserve their single protein water transport rates in biomimetic membranes, while their reconstitution density is variable, leading to different overall membrane permeabilities. It is also shown that membrane protein insertion efficiency inversely correlates with both chemical and physical hydrophobicity mismatch between membrane protein and the membrane matrix.

1. Introduction

Cell membranes separate cell interiors from their environment and are primarily composed of lipids and proteins.[1] Membrane proteins perform the vast majority of the specific functions required for life, including signal reception,[2] material transport[3] and biochemical reactions[4] that occur at the membrane–liquid interface. Success in understanding membrane protein function has led to the use of membrane protein specific properties, such as selective and efficient transport, for developing lipid-based and more recently, polymer-based functional biomimetic membranes.[5] There has also been a rapid increase in the design of synthetic membrane protein mimics[6] and their integration into biomimetic platforms. For instance, as alternatives for aquaporins (AQPs) in biomimetic membranes, bioinspired peptide-appended pillar[*n*]arene channels (PAP channels) were incorporated into lipid vesicles and have been shown to have water transport rates approaching those of AQPs.[6a] They have a structure that mimics membrane

T. Ren, Prof. M. Erbakan, Dr. Y. Shen, E. Barbieri, Dr. P. Saboe, H. Feroz, J. F. Hall, A. B. Schantz, Prof. M. Kumar
Department of Chemical Engineering
The Pennsylvania State University
University Park, PA 16802, USA
E-mail: manish.kumar@psu.edu

Dr. M. Erbakan
Department of Biosystem Engineering
Bozok University
Yozgat 66000, Turkey

E. Barbieri
Departamento de Engenharia Química
Universidade Federal do Rio de Janeiro
Centro de Tecnologia
Bloco E, Rio de Janeiro, RJ CEP 21941-909, Brazil

Dr. H. Yan, S. Ms. McCuskey, Prof. G. C. Bazan
Department of Chemistry and Biochemistry
University of California
Santa Barbara, CA 93106, USA

Prof. P. J. Butler
Department of Biomedical Engineering
The Pennsylvania State University
University Park, PA, USA 16802

Dr. M. Grzelakowsk
Apllied Biomimetic
Cinncinati, OH 45237, USA
E-mail: mg@appliedbiomimetic.com

The ORCID identification number(s) for the author(s) of this article can be found under https://doi.org/10.1002/adbi.201700053.

DOI: 10.1002/adbi.201700053

 © 2017 WILEY-VCH Verlag GmbH & Co. KGaA, Weinheim

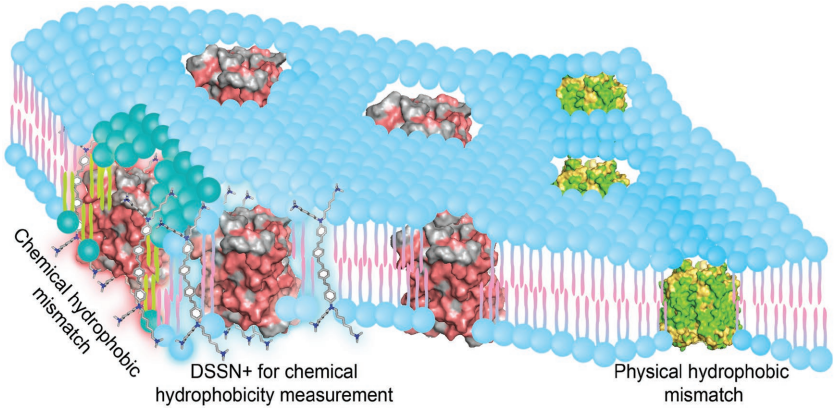
proteins in a simplified manner and can be used as a model for membrane proteins. In particular, the control over the placement of specific membrane facing amino acids provides an ideal model for studying the influence of chemical hydrophobicity mismatch between membrane proteins and biomimetic membranes on the reconstitution process. Membrane protein enhanced biomimetic membranes have been applied to areas such as DNA sequencing,[7] sensing,[8] drug delivery,[9] and water purification.[10] For biomimetic functional materials development, compatibility between lipid (or lipid-like amphilic block copolymer) bilayers and membrane proteins are essential to preserving membrane protein function. High compatibility allows for high protein packing density per unit membrane area and for retention of the native structure and function of proteins. Quantifying and understanding the compatibility between membrane proteins and biomimetic membranes are thus necessary for functional biomimetic materials development.

To better understand compatibility between membrane proteins and membranes, there are three questions that need to be addressed with respect to compatibility: (1) Are specific protein functions being modified after reconstitution into biomimetic membranes? (2) Are there differences in the ability of membrane materials to incorporate a particular membrane protein? (3) What properties of biomimetic materials have the greatest influence on membrane protein compatibility? Here, we propose the following quantitative parameters to address the questions posed above: (1) Average single protein property, such as the average single channel permeability of transport membrane proteins which can be used to quantify whether membrane protein functions have been modified after reconstitution into biomimetic membranes. Compatible biomimetic membranes should not negatively impact the desired average single protein property. (2) Reconstitution density and insertion efficiency: Membrane protein reconstitution density is the number of proteins packed per unit membrane area and can be used to calculate average single protein properties. However, reconstitution density is not an ideal parameter for comparing the protein incorporation ability of different materials, since high reconstitution density may be achieved with high initial protein concentration (most of which do not incorporate in the material) despite low compatibility between the membrane proteins and biomimetic membrane. Instead, we use insertion efficiency, which is the ratio of actual protein reconstitution density to theoretical protein reconstitution density if all proteins were incorporated,[11] to describe the ability of a biomimetic membrane to incorporate proteins, and provide guidance for optimizing protein concentrations for membrane protein incorporation. (3) Hydrophobicity mismatch between membrane proteins and biomimetic membranes: we propose that both physical hydrophobicity mismatch and chemical hydrophobicity mismatch influence membrane proteins' compatibility with biomimetic matrices. Physical hydrophobicity mismatch is the thickness difference (Δd) between membrane protein hydrophobic length (l_0) and bilayer hydrophobic core thickness (d),[12] while chemical hydrophobicity mismatch describes the difference in polarities between membrane protein outer surfaces and biomimetic membrane hydrophobic cores. Minimizing hydrophobicity mismatch will lead to energetically favorable insertion and thus improve membrane protein insertion efficiency.

Recently, we reported values for average single channel permeability and insertion efficiency of the water channel membrane protein, Aquaporin Z from *Rhodobacter sphaeroides* (RsAqpZ),[11] and an artificial water channel mimic, the peptide-appended pillar[5]arene (PAP) channel,[6a] by combining stopped flow light scattering (SFLS) and fluorescence correlation spectroscopy (FCS). SFLS was used to measure bulk permeability (P_f) of protein containing and empty biomimetic membrane vesicles by characterizing the vesicle volume change in hypertonic (or hypotonic) solutions.[13] FCS[14] was applied as in previous studies[6a,11] to measure protein reconstitution density. Average single channel permeability of AqpZ and PAP channel can be calculated from bulk permeability (P_f) and protein reconstitution density. However, to the best of our knowledge, there are no studies focused on water channel compatibility with biomimetic materials. It has been reported that biomimetic membrane water permeability changes nonlinearly with water channel protein concentration[15] and there is a reconstitution limit to membrane proteins in membranes.[16] Studies also report that the decreases in membrane water permeability may occur because the permeability of a single water channel decreases based on different interactions with different membrane materials. For instance, *Escherichia coli* (*E. coli*) AqpZ membrane permeability was reported to decrease in lipid membranes containing cardiolipin.[17] We do emphasize that average single channel permeability was not evaluated in this earlier study on the influence of cardiolipin on AqpZ permeability. Also, it is still unclear how the insertion efficiency and single channel permeability of RsAqpZ and PAP channels would be influenced by properties of different biomimetic membranes.

Here, we studied membrane protein compatibility in different biomimetic membrane matrices and focused on developing a platform for understanding of how biomimetic material properties influence membrane protein compatibility. The bacterial water transport membrane protein—Aquaporin Z, and the artificial water channel—peptide-appended pillar[5]arene (PAP) were reconstituted into several biomimetic materials. We designed and conducted experiments that cover all classes of currently used materials for biomimetic materials research and commercialization including both artificial and biological water channels mentioned above, a natural lipid system (L-α-phosphatidylcholine (PC) and L-α-phosphatidylserine (PS)),[18] and lipid-like amphiphilic block copolymer systems including (poly-(2-methyloxazoline)-poly-(dimethylsiloxane)-poly-(2-methyloxazoline) (PMOXA-PDMS-PMOXA)[10a,19] and poly(butadiene)-*b*-poly(ethylene oxide)(PB-PEO).[5,20] Taking aquaporin (and PAP channel) based biomimetic membranes' transport properties into account, we selected biomimetic materials that showed obvious improvements in water transport properties after protein incorporation, to study their compatibility with membrane proteins. Thus, Aquaporin Z proteins were incorporated into natural lipid systems and the PMOXA-PDMS-PMOXA block copolymer system, while PAP channels were incorporated into natural lipid systems and the PB-PEO block copolymer system.

© 2017 WILEY-VCH Verlag GmbH & Co. KGaA, Weinheim



Scheme 1. Chemical hydrophobicity mismatch and physical hydrophobicity mismatch are the two key factors that influence membrane protein compatibility with biomimetic membranes, and are measurable using techniques described in this paper. We measured the hydrophobic mismatch (both chemical and physical) in membrane protein reconstituted biomimetic membranes, and assessed their influence on membrane protein insertion efficiency. Here, chemical hydrophobic mismatch describes the difference in hydrophobic character between membrane protein outer surfaces and biomimetic membrane hydrophobic cores. Chemical hydrophobic mismatch is measured using a distyrylbenzene chromophore (DSSN+) based assay presented in this paper, while physical hydrophobicity mismatch is the thickness difference (Δd) between membrane protein hydrophobic length l_0 and bilayer hydrophobic core length (d).

Average single channel permeability and insertion efficiency of water channels were measured through combination of SFLS and FCS. For further investigation into how hydrophobicity mismatch influences membrane protein compatibility, we characterized and discussed both physical hydrophobicity mismatch and chemical hydrophobicity mismatch as shown in **Scheme 1**. Physical hydrophobicity mismatch can be calculated as the hydrophobic thickness difference between membrane protein hydrophobic length and the bilayer hydrophobic core length.[21] Bilayer hydrophobic core lengths were calculated based on previously reported bilayer hydrophobic core thickness data that were obtained from Cryo-EM images of block copolymer vesicles[22] (see details in Table S1 and Figure S1 in the Supporting Information). For chemical hydrophobicity mismatch determination, we developed a novel approach. We used a membrane-intercalating fluorophore that is sensitive to solvent polarity: 4,4′-bis(4′-(*N*,*N*-bis(6″-(*N*,*N*,*N*-trimethylammonium)hexyl)amino)-styryl)stilbene tetraiodide (DSSN+).[19] In general, at a fixed absorbance wavelength, when solvent polarity increases, there is a red shift in the DSSN+ emission peak, indicating that DSSN+ in a more polar solvent needs less energy to stabilize its structure.[20] Applying the same concept to biomimetic membrane systems, we reconstituted DSSN+ into vesicle based biomimetic membranes and used DSSN+ emission spectra to indicate the polarity of hydrophobic cores of biomimetic membranes. We further propose the use of polarity change induced by membrane protein incorporation into biomimetic membranes as a measure of the chemical hydrophobicity mismatch between the protein and the membrane. This work presents, for the first time, measurements of chemical hydrophobicity mismatch between biomimetic materials and membrane proteins, and elaborates upon the influence of chemical hydrophobicity mismatch on membrane protein-matrix compatibility in biomimetic membranes.

2. Results and Discussions

2.1. Measurement of RsAqpZ Reconstitution Density and Single Channel Permeability in Biomimetic Materials

The bacterial water channel protein, Aquaporin Z (AqpZ) has been used as a model membrane protein that can be functionally incorporated into several lipid and polymer biomimetic membranes,[10,15,21] and bulk permeability differences of AqpZ based vesicles in different biomimetic membranes have been widely discussed in previous studies.[22] Here, we reconstituted RsAqpZ (overexpressed in *E. coli* expression system)[23] into several biomimetic membranes (including lipids and block copolymers) at various membrane matrix (lipid or polymer) to protein ratios (LPR is short for lipid to protein ratio, PoPR is short for polymer to protein ratio in this paper) to investigate how the selection of biomimetic membranes influences RsAqpZ reconstitution density and average single channel permeability. To provide comparable conditions for RsAqpZ in different biomimetic membranes, we optimized detergent selection and detergent concentration during RsAqpZ reconstitution process. In all cases we used preformed vesicles in and then added detergent solubilized RsAqpZ. We used appropriate concentrations of compatible detergents to "loosen" the vesicles while keeping RsAqpZ stable. While octyl glucoside (OG) at 0.7% was found to be appropriate to loosen polymers while keeping proteins stable, 0.3% decyl maltoside was found appropriate to loosen lipid vesicles while keeping proteins stable.

The biomimetic membranes chosen included both lipids and PMOXA-PDMS-PMOXA block copolymers. RsAqpZ was first reconstituted into PC/PS (4:1 mol:mol) lipid vesicles at several lipid to protein mass ratios (wLPR) with fixed initial lipid concentrations, and the net permeability of the proteoliposome (proteoliposome permeability – empty vesicle permeability) was measured using SFLS. As shown in **Figure 1**A, when normalized light scattering curves obtained from SFLS are compared, AqpZ reconstituted vesicles show faster kinetics than non-protein reconstituted vesicles (control), indicating that water transport is faster in protein-reconstituted vesicle samples. In addition, as initial protein concentration increased (reflected in decreasing wLPR values), normalized light scattering curves had increasing initial exponential rates of rise, k. We calculated net permeability of vesicles based on k (see details in the Experimental Section), and found that the net permeability increased nonlinearly as the initial protein concentration increased (Figure 1B). For instance, initial protein concentration of LPR24 sample was 15 times that of LPR360, while net permeability of LPR24 sample was only approximately four times that of LPR360 samples. In order to calculate the actual number of proteins incorporated per vesicle and the permeability per protein, we conducted an FCS-based evaluation pioneered by Pohl and co-workers[14] and used previously for RsAqpZ.[11] Although

© 2017 WILEY-VCH Verlag GmbH & Co. KGaA, Weinheim

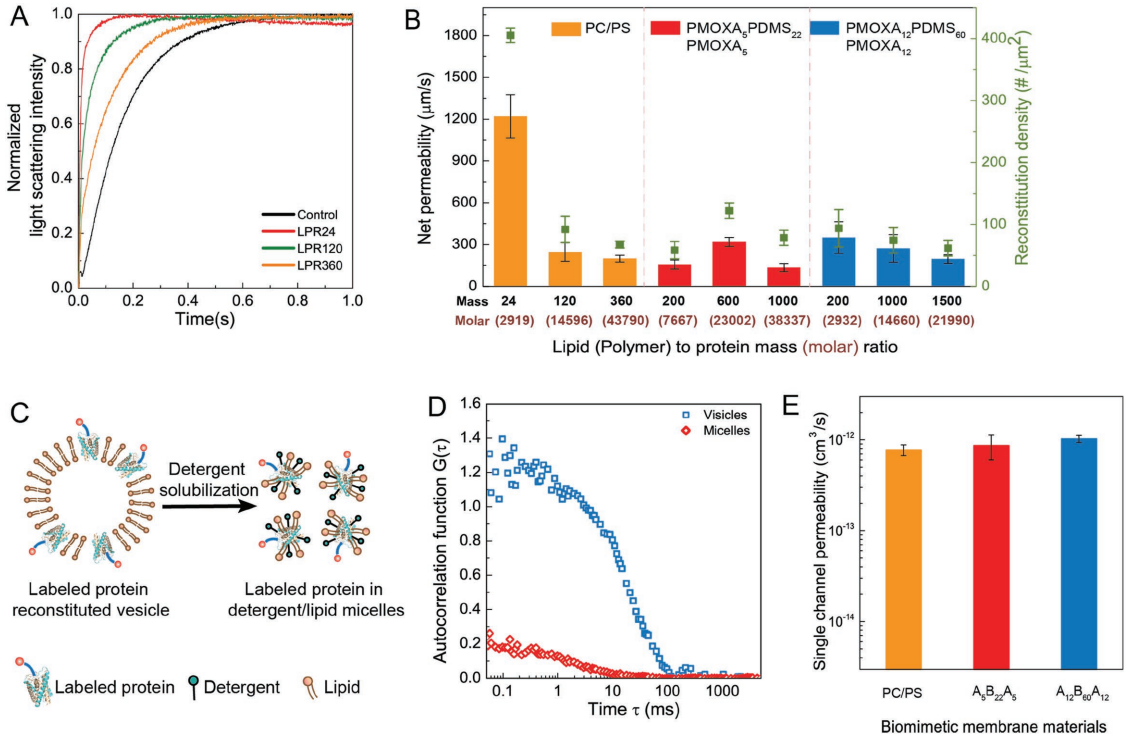


Figure 1. Changes in permeability of reconstituted membrane with changing initial protein concentrations result from changes in reconstitution density of RsAqpZ. A) Stopped flow traces from experiments performed on RsAqpZ reconstituted lipid vesicles. Change in the rate of light scattering increase indicates changing permeability. B) RsAqpZ-reconstituted lipid and block copolymer membrane net permeability (bars) and RsAqpZ reconstitution density (points) change at different lipid to protein ratios. C) FCS was used to determine the number of proteins per vesicle (N_{pro}/N_{ves}). First, FCS was used to count the number of labeled protein reconstituted vesicles (N_{ves}), then vesicles were broken down into micelles by adding detergent to the vesicle solutions, and we calculated the number of labeled protein micelles (N_{pro}) from FCS. D) FCS autocorrelation functions for RsAqpZ reconstituted vesicles and RsAqpZ micelles. The y-intercept of each curve represents the inverse of the number of diffusing fluorescent particles in the confocal volume. E) RsAqpZ single channel water permeability in the different biomimetic membranes tested did not show significantly different values. $A_{12}B_{60}A_{12}$ is the abbreviation used for block copolymer $PMOXA_{12}PDMS_{60}PMOXA_{12}$, and $A_5B_{22}A_5$ is the abbreviation used for block copolymer $PMOXA_5PDMS_{22}PMOXA_5$.

protein fusions with fluorescent proteins have been used in the past,[11] in this study we developed a chemical labeling technique to allow for more flexibility in working across a wide range of proteins. We selected a label that can be linked with the protein primary amines in aqueous solution and only generated fluorescence signal after it was conjugated with the protein, and the labeling process had little influence on RsAqpZ activity (see details in Figure S2 in the Supporting Information). The dye used was a pyrylium dye (Chromeo P540 Py-Dye, Active Motif Inc.), which has a maximum emission wavelength of 623 nm. Pyrylium dye labeled RsAqpZ was then reconstituted into PC/PS vesicles. As shown in Figure 1C, we first performed FCS on labeled protein reconstituted vesicles, and the number of vesicles (N_{ves}) was counted by fitting the autocorrelation function curve obtained from FCS. After detergent addition to the vesicle solutions, the vesicles broke down into labeled protein-detergent-lipid/polymer micelles. The number of proteins (N_{pro}) was obtained from FCS using the same fitting method. Based on previous studies, at a final octyl glucoside (OG) concentration of 2.5% (wt/vol), we concluded that there was one protein tetramer per micelle.[11,24] By taking the ratio of N_{pro}/N_{ves}, we calculated the number of proteins per vesicle and RsAqpZ reconstitution density in different materials. Because free dye signal was not detectable, we were able to perform single species fitting for the autocorrelation function obtained from FCS. As shown in Figure 1D, the diffusion time of RsAqpZ reconstituted vesicles was longer (as seen from the shape of the curve, with estimated diffusion times at values corresponding to half of the y-intercept) than that of RsAqpZ micelles formed after adding detergent to vesicles. The difference in diffusion time was mainly caused by the size difference between vesicles and micelles. In the same material, as initial protein concentration increased, the trend of reconstitution density change was the same as the trend of permeability change (Figure 1B). Using the vesicles' net permeability and protein reconstitution density (directly measured from experiment), we calculated RsAqpZ average single channel permeability in the lipid membrane as 7.8 ($\pm$ 1.1) $\times 10^{-13}$ cm^3 s^{-1}, corresponding to a transport rate of 2.6 ($\pm$ 0.3) $\times 10^{10}$ water molecules per second, which is in close agreement with a previous report[11] on this protein.

After measuring RsAqpZ reconstitution density and single channel permeability in lipid vesicles, we reconstituted RsAqpZ into lipid-like amphiphilic block polymers, PMOXA-PDMS-PMOXA, at different polymer to protein mass ratios (wPoPR) to compare RsAqpZ reconstitution density and single channel permeability in block copolymer

© 2017 WILEY-VCH Verlag GmbH & Co. KGaA, Weinheim

membranes. PMOXA-PDMS-PMOXA is a widely used biomimetic membrane material that been demonstrated to successfully reconstitute AqpZ and other membrane proteins in previous studies.[10a,21,25] In addition, PMOXA-PDMS-PMOXA has higher chemical and mechanical stability compared to lipids, so it is a material being used for development of AqpZ based desalination membranes.[10a,26] Polymer (or lipid) to protein molar ratios (mPoPR or mLPR) were maintained in similar ranges (see details in Table S2 in the Supporting Information), with lipids at mLPR 3000–46 000, $PMOXA_{12}PDMS_{60}$ $PMOXA_{12}$ at mPoPr 3000–23 000, and $PMOXA_5PDMS_{22}$ $PMOXA_5$ at mPoPr 8000–40 000). As shown in Figure 1B, in the same block copolymer membranes, reconstitution density change followed the same trend as net permeability change. However, comparing different block copolymers, the trends in reconstitution density change were different: protein reconstitution density increased nonlinearly as initial protein concentration increased in $PMOXA_5PDMS_{22}PMOXA_5$ vesicles, while in $PMOXA_{12}PDMS_{60}PMOXA_{12}$ vesicles, protein reconstitution density first increased then decreased as initial protein concentration increased. The decrease of protein reconstitution density when initial protein concentration increased at higher initial protein concentration conditions (reflected as lower mPoPR in the figure) may be because at high protein concentrations, aggregation occurs when there are large numbers of proteins that cannot be reconstituted into vesicles and the exact trend depends on the protein reconstitution efficiency of the polymer and the added protein concentration. These results demonstrate that the abilities of biomimetic membranes to incorporate RsAqpZ were not the same among different materials, and that increasing initial protein concentration did not increase reconstitution density monotonically for all biomimetic materials. However, single channel permeability in different materials remained constant, indicating that RsAqpZ single protein property is not modified after incorporation into the different materials tested. The overall average single channel permeability determined was 8.9 (± 1.9) × 10^{-13} cm^3 s^{-1}, corresponding to a transport rate of 3.0 (± 0.6) × 10^{10} water molecules per second (Figure 1E).

2.2. Measurement of Pillar[*n*]arene Channels Reconstitution Density and Single Channel Permeability in Biomimetic Materials

Pillar[*n*]arene channels have been developed as synthetic artificial channels that can mimic aquaporins properties.[6a,b] Though PAP channels' insertion efficiency and single channel permeability in PC/PS lipids have been reported,[6a] the effects of biomimetic membrane differences on PAP channel compatibility are still not known. Here, we reconstituted PAP channels into three lipid systems: the PC lipid system, the PC/PS (4:1 mol:mol) lipid system, and the PC/PS/cholesterol (CHL) (4:1:5 mol:mol:mol) lipid system. PC lipids have been widely applied to membrane protein studies and showed successful incorporation of a range of membrane proteins.[18b,27] Based on our previous work, by adding PS lipids (which is negatively charged) to the PC lipid system, the stability of the lipid vesicles is increased.[11] In addition, we also chose to add cholesterol to the lipid system to mimic certain biological membrane systems where cholesterol is found in abundance. PAP channel membrane osmotic water permeability was measured under hypotonic shock, as was done in the previous study.[6a] As seen in **Figure 2**A,B, light scattering values decreased over time for vesicles with PAP channels exposed to hypotonic solution, indicating swelling of vesicles. Comparing light scattering curves between PAP channel reconstituted samples and control samples, for the PC lipid system, stopped flow light scattering curves of from PAP channel reconstituted samples decreased faster than those of control vesicles (Figure 2A). This indicated that the vesicle bulk permeability increased due to the contribution of PAP channels in the vesicles. However, in PC/PS/CHL lipids, the light scattering curve of PAP channel reconstituted vesicles decreased at similar rate compared to that of control vesicles, showing no measurable bulk permeability difference between PAP channel reconstituted vesicles and control vesicles (Figure 2B) indicating no insertion of channels. We calculated the net permeability of all the samples (Figure 2C) with various lipids containing PAP channels incubated to achieve the same lipid to channel molar ratio (mLPR) before insertion. Each

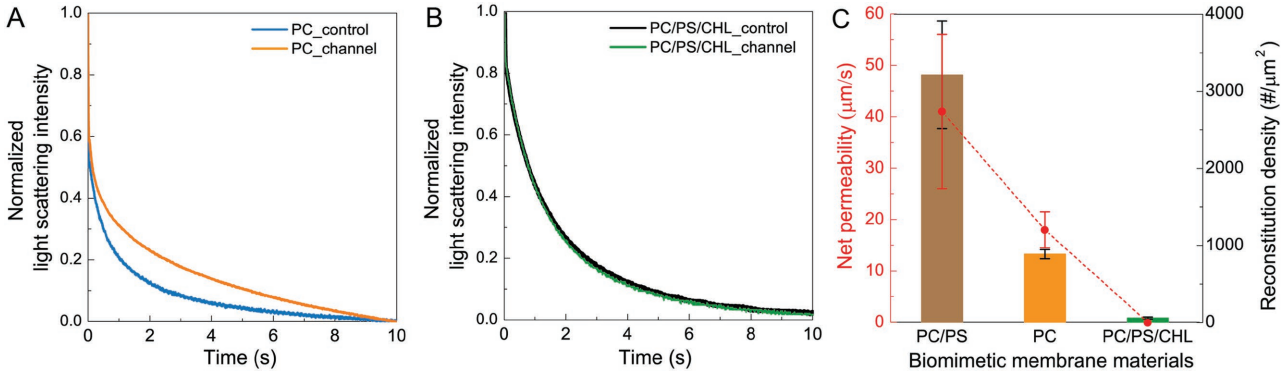


Figure 2. The proposed compatibility platform provides information on reconstitution density and single channel permeability for the artificial water channel, PAP, in different matrices. A) Stopped flow traces of experiments performed on PC vesicles with reconstituted PAP channels, showing permeability differences between control vesicles and PAP channel reconstituted vesicles. B) Stopped flow traces from experiments performed on PC/PS/CHL vesicles with reconstituted PAP channels, showing no permeability differences between control vesicles and PAP channel reconstituted vesicles. C) Net permeabilities (points) of lipid membranes with reconstituted PAP channels and reconstitution density changes (bars) in different biomimetic materials.

© 2017 WILEY-VCH Verlag GmbH & Co. KGaA, Weinheim

combination of lipid with channels at the same LPR resulted in a different net permeability: PAP reconstituted PC/PS vesicles had the highest net permeability, while PAP reconstituted PC/PS/CHL vesicles showed no detectable net permeability from channels. We also performed FCS experiments to calculate PAP channel reconstitution density (Figure 2C). The results from these experiments show that PC/PS vesicles had the highest PAP channel reconstitution density, which is close to 60 times of PAP channel reconstitution density in PC/PS/CHL system. Similar to the calculations for RsAqpZ, average single channel permeability of PAP channel was calculated based on net permeability and reconstitution density. Average single channel permeability of PAP channel in the PC/PS lipid system is 1.8(± 0.4) × 10^{-14} cm^3 s^{-1}, while in PC lipid system is 2.0(± 0.5) × 10^{-14} cm^3 s^{-1}, indicating average single channel permeability of PAP channel remained constant in the different lipid systems (except the PC/PS/CHL system where there was no significant incorporation), though PAP channel insertion is affected greatly. Single channel permeability of PAP channels in PC/PS/CHL was not calculated, as net permeability was not measureable due to the low reconstitution density of PAP channels in PC/PS/CHL system. When cholesterol is added to a lipid system it leads to a lowering of the fluidity of the membrane,[28] and/or change in the hydrophobicity of the membrane interior, which may make it more difficult for PAP channel to insert into biomimetic membranes and lead to the low reconstitution density of PAP channels seen in PC/PS/CHL system.

2.3. Single Channel Permeability of AqpZ Homologs, Fusions, and Artificial Water Channels

Using RsAqpZ and PAP channels as examples, we compared their reconstitution density and average single channel permeability in different biomimetic membranes. Though the biomimetic membranes had differences in their ability to incorporate membrane proteins, for the same membrane protein, the single channel permeability was similar in the different biomimetic membranes tested, demonstrating the utility of the proposed platform in testing matrix effects on incorporation efficiency and biophysical transport properties. Further, to demonstrate the utility of this platform for identifying differences between proteins (e.g., to select the most permeable of several homologous proteins for use in a biomimetic membrane), we used this platform to compare the single-channel permeabilities of AqpZ homologs and fusions. These results are summarized in **Figure 3**. AqpZ homologs and fusions included a gene fusion of RsAqpZ with a derived fluorescent tag (labeled as RsAqpZ_mBanana in Figure 3), untagged RsAqpZ (labeled as RsAqpZ in Figure 3), *E. coli* AqpZ (labeled as EcAqpZ in Figure 3), and the synthetic water channel analog PAP channel (labeled as PAP channel in Figure 3). Clear differences in single channel water permeability among different AqpZ homologs and fusions could be discerned, revealing the following trend: RsAqpZ_mBanana = RsAqpZ > EcAqpZ > PAP channel.

In addition to the bacterial water channels AQPs and their mimics, we also explored the ability of the proposed techniques to evaluate the incorporation of light driven chloride channels,

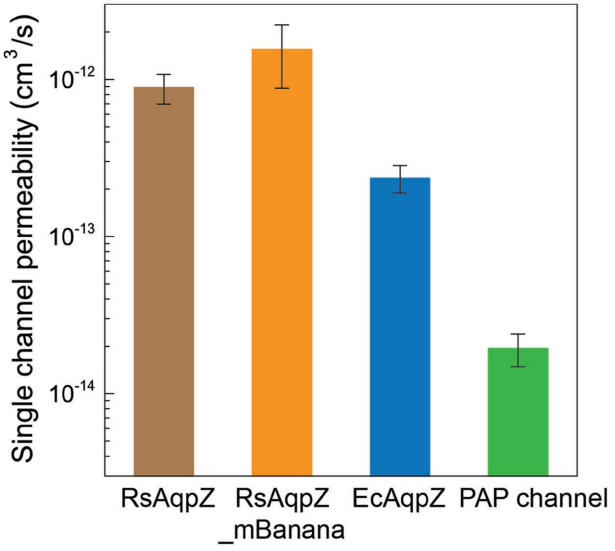


Figure 3. Single channel permeability differences among AqpZ homologs, fusions, and artificial channels are clearly discernable using the proposed platform. Single channel permeability summary of AqpZ homologs, AqpZ fusions, and PAP channels using the proposed platform indicates its utility in comparing intrinsic permeabilities of water channels to elucidate the effect of protein tags, organism of origin, and between artificial and biological channels.

halorhodopsins (pHR) in biomimetic matrices. These light driven channels have potential applications as optogenetic tools[29] for neurobiology research. Here, we applied our compatibility platform to pHR to accurately measure reconstitution density to provide information for calculating single protein transport rates (see details in Table S3 in the Supporting Information).

2.4. Measurement of Biomimetic Membranes Hydrophobicity Mismatch with Membrane Proteins

Biomimetic membranes had differences in their ability to incorporate membranes proteins, which may relate to their chemical and physical hydrophobicity mismatch with the membrane proteins. Here, we use insertion efficiency, which is defined as the ratio of actual protein reconstitution density to theoretical protein reconstitution density,[11] instead of reconstitution density to represent the biomimetic membranes' ability to incorporate membrane proteins, and discuss how hydrophobicity mismatch influences membrane protein insertion efficiency. Actual protein reconstitution density can be measured by FCS, while theoretical protein reconstitution density is calculated based on membrane area occupied by each lipid or polymer and initial protein concentration.

Previous studies have shown that when a hydrophobic thickness mismatch exists between the protein's hydrophobic band and the hydrophobic thickness of the biomimetic membrane,[30] it exposes the membrane protein's hydrophobic residues to aqueous solutions or hydrophilic residues to the hydrophobic lipid bilayer core. This imposes an energetic penalty, which makes it more difficult for membrane proteins to

© 2017 WILEY-VCH Verlag GmbH & Co. KGaA, Weinheim

be reconstituted into bilayers and bilayer-like membranes.[12] To compensate for this physical hydrophobicity mismatch, block copolymers near membrane proteins can undergo a structural change in thickness to match membrane protein hydrophobic length.[31] Using a PC/PS lipid bilayer as a reference, we compared the RsAqpZ insertion efficiency range in PMOXA-PDMS-PMOXA (ABA) membranes with different hydrophobic thicknesses. We used $PMOXA_5PDMS_{22}PMOXA_5$ and $PMOXA_{12}PDMS_{60}PMOXA_{12}$ with hydrophobic thicknesses of 4.4 and 9.0 nm, respectively, estimated based on reported ABA hydrophobic thickness.[32] Because AqpZ hydrophobic band thickness was estimated as 3 nm based on its crystal structure,[30a] the physical hydrophobicity mismatch between AqpZ and bilayers had the following sequence: PC/PS ($\Delta d = 1$ nm) < $PMOXA_5PDMS_{22}PMOXA_5$ ($\Delta d = 1.4$ nm) < $PMOXA_{12}PDMS_{60}PMOXA_{12}$ (Δd = 6 nm). The overall range of RsAqpZ insertion efficiencies, at a range of PoPRs, in $PMOXA_5PDMS_{22}PMOXA_5$ is higher than that of RsAqpZ in $PMOXA_{12}PDMS_{60}PMOXA_{12}$, indicating that minimizing hydrophobicity thickness mismatch results in an increase in the insertion efficiency (see details in Figure S3 in the Supporting Information).

In addition to the physical hydrophobicity mismatch discussed above, we propose chemical hydrophobicity mismatch, or more specifically, polarity mismatch between the membrane protein outer surface and the hydrophobic cores of biomimetic membranes also influences membrane protein insertion efficiency in biomimetic membranes. Since membrane proteins can be thought of as polymer molecules with hydrophobic transmembrane sections, membrane protein reconstituted biomimetic membrane matrices can be regarded as a mixture of two kinds of polymers, lipids (or lipid-like polymers) and membrane proteins.

Based on the Flory–Huggins theory, similarity in hydrophobicity between polymers (often quantified by Hildebrand solubility parameter) will decrease the Flory–Huggins interaction parameter (χ_{AB} in Equation (1))[33]

$$\chi_{AB} = \frac{V_r}{RT}(\delta_A - \delta_B)^2 \quad (1)$$

where V_r is reference volume (molar volume of the smallest repeat unit), R is the ideal gas constant, T is temperature, and δ is the solubility parameter of polymer A or B as indicated by the subscript.

A decrease in the Flory–Huggins interaction parameter leads to a decrease in the Gibbs free energy of mixing between the two polymers as shown by the Flory–Huggins equation (Equation (2))[33]

$$\frac{\Delta G_{mix}}{VRT} = \frac{\phi_A}{V_A}\ln\phi_A + \frac{\phi_B}{V_B}\ln\phi_B + \frac{\chi_{AB}\,\phi_A\phi_B}{\sqrt{V_A V_B}} \quad (2)$$

where ΔG_{mix} is free energy of mixing, V is the total volume, R is the ideal gas constant, T is temperature, and δ is the solubility parameter, ϕ_i is volume fraction of i, V_i is molar volume of i, χ_{AB} is Flory–Huggins interaction parameter.

Thus, decreasing the chemical hydrophobicity mismatch between the protein's outer surface and the biomimetic membrane's hydrophobic core will lead to energetically favorable insertion of the membrane proteins into the membrane. We used the hydrophobicity probe DSSN+ to characterize bilayer membrane hydrophobicity and developed a method to compare chemical hydrophobicity mismatch between membrane proteins and membranes using different biomimetic membrane-PAP channel systems as models.

As stated earlier, the emission spectra of DSSN+ have been used previously to characterize solvent polarity. Solvent polarity's influences on DSSN+ emission spectra can be described by the Lippert equation[20] (Equation (3))

$$\frac{1}{\lambda_A} - \frac{1}{\lambda_F} = \frac{2}{hc}\left[\frac{\varepsilon - 1}{2\varepsilon + 1} - \frac{n^2 - 1}{2n^2 + 1}\right]\frac{[M_E - M_G]^2}{a^3} + \text{constant} \quad (3)$$

where λ_A is wavelength of absorbance, λ_F is wavelength of emission, h is Planck's constant, c is the speed of light, a is the radius of cavity where fluorophore resides, ε is dielectric constant of solvent, n is refractive index of solvent, M_E is the fluorophore excited state dipole moment , and M_G is the fluorophore ground state dipole moment.

Because solvent dipoles can rearrange to stabilize charge separation in DSSN+'s excited state, the energy released upon relaxation from the excited to the ground state decreases as solvent polarity increases. This results in an emission peak wavelength increase (a red shift). We tested the ability of DSSN+ to respond to various solvents with known polarity (represented by their dielectric constant), including toluene, tetrahydrofuran, dichloromethane, acetone, dimethyl sulfoxide, and water. As shown in **Figure 4**A, as expected, wavelength of DSSN+ emission peak (λ_{em}) showed a large blue shift as solvent polarity decreased. Using the wavelength of the DSSN+ emission peak in water as a reference, we plotted this shift as a function of the solvent's dielectric constant (Figure 4B), confirming that there was a general increase in blue shift as the polarity of the solvent, and thus the dielectric constant, decreased. It has also been reported that DSSN+ spontaneously inserts into the hydrophobic section of the lipid bilayer with a resulting emission peak shift similar to that seen in organic solvents.[19] In this work, DSSN+ was added to different biomimetic membrane vesicles, including PC/PS liposomes, PMOXA-PDMS-PMOXA polymersomes, and PB-PEO polymersomes. By normalizing the emission spectra of DSSN+ in different biomimetic membrane vesicles, we observed different DSSN+ emission peak shifts (Figure 4C). Using the wavelength of the DSSN+ emission peak in the vesicle rehydration buffer (HEPES buffer) as a reference, DSSN+ emission peak wavelength shifts in different biomimetic membranes had the following sequence: $|\Delta\lambda_{em,PC/PS}| \gg |\Delta\lambda_{em,PDMS}| > |\Delta\lambda_{em,PB}|$ (Figure 4D). Based on the magnitude of these shifts and their relative trends, we propose that biomimetic membrane hydrophobicity has the following trend for commonly used matrices: PC/PS > PDMS > PB.

With success in using DSSN+ to easily compare the hydrophobicities of different biomimetic membrane cores, we further hypothesized that if membrane proteins were added to the biomimetic membrane with DSSN+, the modulation of emission shift will indicate hydrophobicity change of biomimetic membrane matrices, which is caused by the existence of chemical hydrophobicity mismatch between membrane protein and

© 2017 WILEY-VCH Verlag GmbH & Co. KGaA, Weinheim

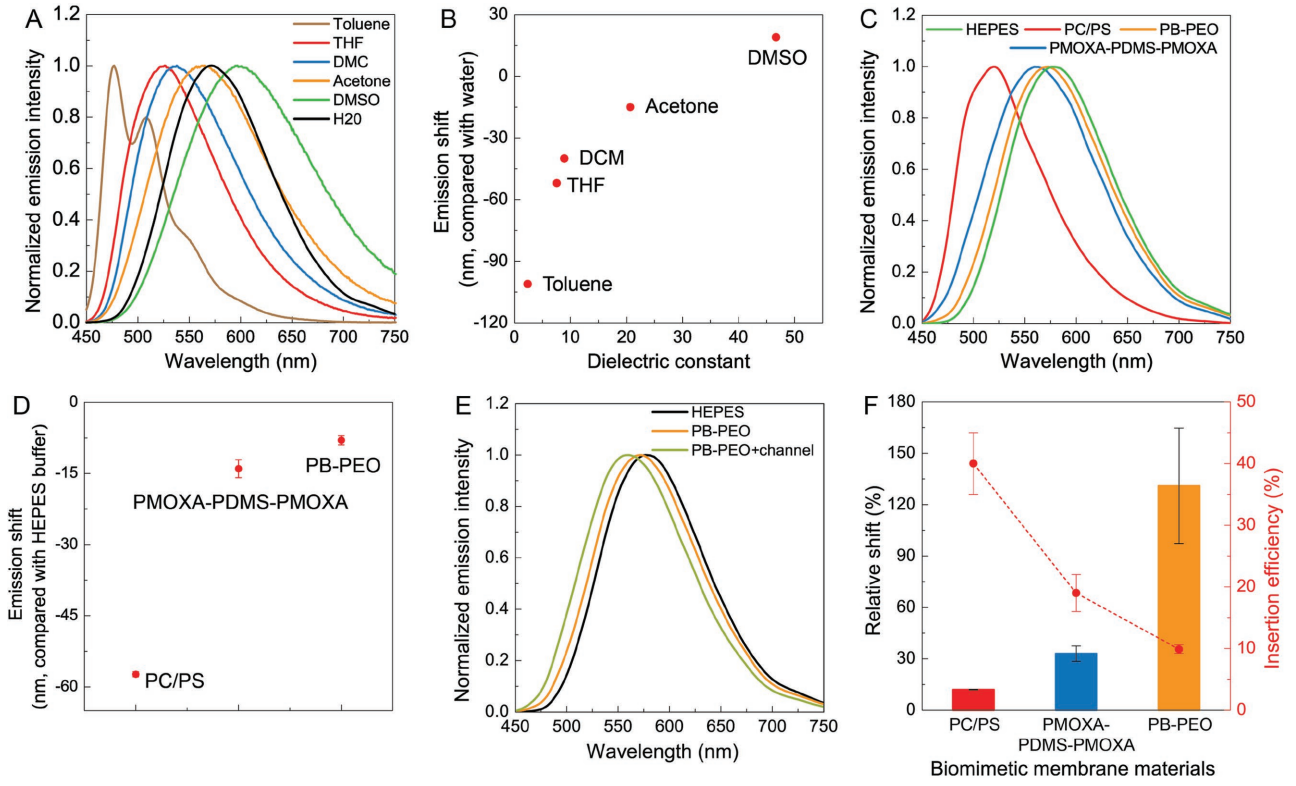


Figure 4. The membrane intercalating fluorophore, 4,4′-bis(4′-(*N*,*N*-bis(6″-(*N*,*N*,*N*-trimethylammonium)hexyl)amino)-styryl)stilbene tetraiodide (DSSN+), changes its emission wavelength maximum based on its environment. This change can be used to evaluate the hydrophobicity of biomimetic membrane core regions. A) Normalized DSSN+ emission spectra in solvents with different hydrophobicities (indicated by the dielectric constant). B) Because solvent dipoles can rearrange to stabilize charge separation in DSSN+'s excited state, the energy released upon relaxation from the excited to the ground state decreases as solvent polarity increases. This results in an emission peak wavelength increase (a red shift). C) Normalized DSSN+ emission spectra in different biomimetic membranes. D) DSSN+ maximum emission wavelength shift in different biomimetic membranes from the DSSN+ maximum emission wavelength in buffer. E) Normalized DSSN+ emission spectra in PB-PEO vesicles after PAP channel reconstitution. The DSSN+ emission shift after PAP channel incorporation into the biomimetic membranes indicates a change in the hydrophobicity of the biomimetic matrices due to incorporation of the channels. F) Relative shift in DSSN+ emission wavelength, and PAP channel insertion efficiency, in different biomimetic materials. The relative shift can be considered a measure of hydrophobic mismatch between the channels (or proteins) and the membrane.

biomimetic membranes. Using PAP channels as a simplified model of membrane proteins, we characterized DSSN+ emission peak wavelength shift when mixing DSSN+ with PAP channel reconstituted biomimetic vesicles, including PC/PS vesicles, PMOXA-PDMS-PMOXA vesicles, and PB-PEO vesicles. PB-PEO was included in this part since is another block copolymer that has been shown to successfully reconstitute membrane proteins.[34] PAP channels were reconstituted into biomimetic vesicles at the same lipid (or polymer) to channel molar ratio. As expected, DSSN+ emission peak wavelength shift between PAP channel reconstituted PB-PEO vesicles and control vesicles were different (Figure 4E). To compare the differences, we defined the parameter relative emission peak shift (Equation (4))

$$\text{relative shift}\,(\%) = \frac{\left|\Delta\lambda_{\text{em,channel}} - \Delta\lambda_{\text{em,control}}\right|}{\left|\Delta\lambda_{\text{em,control}}\right|} \quad (4)$$

where $\Delta\lambda_{\text{em,channel}}$ is the DSSN maximum emission blue shift of the channel reconstituted biomimetic membranes (using HEPES buffer maximum emission wavelength as reference).

We propose that the relative shift could be used as a parameter that describes the hydrophobicity change caused by adding artificial water channels. High relative shift indicates a large hydrophobicity change in the biomimetic membrane matrices, which occurs upon incorporation of channels with a hydrophobicity significantly different from that of the membrane material. As shown in Figure 4F, the relative emission shift in biomimetic membranes induced by the PAP channel had the following sequence: PB-PEO>PMOXA-PDMS-PMOXA>PC/PS. This trend in fluorescence shift is the opposite of the trend observed for insertion efficiency in biomimetic membranes (PB-PEO < PMOXA-PDMS-PMOXA<PC/PS), which verifies our hypothesis that a low chemical hydrophobicity mismatch (small relative shift) correlates with high insertion efficiency.

3. Conclusion

Overall, we have developed a platform to accurately measure protein-membrane compatibility, protein reconstitution

© 2017 WILEY-VCH Verlag GmbH & Co. KGaA, Weinheim

density, insertion efficiency, and average single-protein properties. Using this platform, we found that (i) the biomimetic membranes we tested here had little influence on single channel permeability of AqpZs and PAP channels, the same platform can be used to accurately quantify subtle differences in activities of proteins in different matrices when they arise, (ii) insertion efficiency and reconstitution density both strongly depended on the biomimetic membranes used, both for membrane proteins and for artificial water channels, and (iii) biomimetic membranes' properties (both chemical and physical) have little influence on the activities of the membrane proteins we tested in this paper. However, high insertion efficiency requires that the membrane's hydrophobic core and the protein's outer surface have similar hydrophobic properties (in terms of both hydrophobic thickness and polarity). In this study, we cover all the reported systems that have demonstrated convincing membrane protein insertion including PDMS-PMOXA polymers, PB-PEO polymers, and lipids. We have also tested two versions of aquaporins, artificial water channels and also included rhodopsins. In general, the findings we reported here are representative of biomimetic membranes.

4. Experimental Section

Vesicle Permeability Measurement Using SFLS: AqpZ-reconstituted vesicle permeability was estimated using experiments on a SFLS instrument,[11] following a well-established protocol for aquaporin permeability measurements. Vesicles were rapidly mixed with a high salt concentration osmotic agent (20×10^{-3} M HEPES, 400×10^{-3} M NaCl, 0.02% (wt/vol) NaN3, pH7.4) in the mixing cell of this instrument. Due to the presence of hypertonic solution outside, vesicles shrunk and generated increasing light scattering signals at a 90° angle. Normalized light scattering signal curves were fitted to a double-exponential equation and provided two rate constants,[10a] of which the higher rate constant k represents shrinkage kinetics due to AQP permeability.[13] The rate constant k can be used to calculate water permeability (P_f), following Equation (5) below[10a,13]

$$P_f = \frac{k}{\frac{S}{V_o} \times \Delta\pi \times V_w} \tag{5}$$

where S is surface area of vesicle, V_o is volume of vesicle, $\Delta\pi$ is osmotic pressure gradient, and V_w is molar volume of water.

PAP channel reconstituted vesicles' permeability was also tested using SFLS.[6a] Vesicles were rapidly mixed with hypotonic solutions instead of hypertonic solution, so that vesicles swelled and generated decreasing light scattering signals at a 90° angle. The rate constant k could also be fitted to the light scattering signal curve and used to calculate the PAP channel reconstituted vesicles water permeability using Equation (5).

FCS Determination of Membrane Protein (or Membrane Protein Mimic) Reconstitution Density: Several current methods, including SDS-polyacrylamide gel electrophoresis,[35] UV–vis spectroscopy,[36] and atomic force microscopy,[37] can be used for estimating reconstitution density. However, these methods are semiquantitative at best and reconstitution density at the molecular level cannot be reliably obtained. Thus, to more precisely measure reconstitution density, FCS[14] was applied in previous studies.[6a,11] FCS compares the fluorescence intensity self-similarity property of the confocal volume at time t with time $(t + \tau)$ as a function of lag time τ. The fluorescent particle diffusion coefficient and concentration influence fluorescence signal self-similarity. Fluorescence signal self-similarity properties can be expressed as an autocorrelation function,[38] $G(\tau)$ (Equation (6))

$$G(\tau) = \frac{1}{N}\left[\frac{1}{1+(\tau/\tau_D)}\right]\left[\frac{1}{1+(r/z)^2(\tau/\tau_D)}\right]^{1/2} \tag{6}$$

where τ_D is the 3D lateral diffusion time of fluorescent particles in the confocal volume, and r and z are minor axis and major axis of confocal volume. When $\tau = 0$, $G(\tau) = 1/N$, where N is the average fluorescent particle number in confocal volume.

Here, FCS was used to detect the number of membrane proteins incorporated per vesicle.[11,14] Membrane proteins and protein mimics were either expressed with fluorescent tags or fluorescently labeled by chemical reactions, and reconstituted into vesicles. FCS was conducted on a time correlated single photon counting system at a wavelength of 532 nm as reported previously by the group.[11] Briefly, 50 nm standard fluorescent beads were used for confocal volume system calibration. Vesicle samples were diluted by a certain ratio for FCS detection. The number of vesicles (N_{ves}) in the confocal volume can be estimated from the y-intercept of autocorrelation function of the time-dependent fluorescence signal. HEPES buffer and OG buffer (final OG concentration is 2.5 wt%)[11] were then added to the intact vesicle solution and break down vesicles into micelles. FCS was performed on detergent-protein micelle solutions and obtained the number of protein containing micelles (N_{pro}) in the confocal volume by using the y-intercept of the new autocorrelation function obtained from fluorescent intensity traces of the solubilized micelles. Average number of proteins per vesicle was obtained by taking the ratio N_{pro}/N_{ves}. This ratio, combined with vesicle diameter characterized by dynamic light scattering, allows us to calculate protein reconstitution density.

4,4′-Bis(4′-(N,N-bis(6″-(N,N,N-trimethylammonium)hexyl)amino)-styryl)stilbene tetraiodide (DSSN+) Incorporation in Biomimetic Membranes and Optical Characterization of DSSN+: Vesicles were first diluted to 3 mg mL^{-1} with rehydration buffer and mixed with DSSN+ (1×10^{-3} M, in water) at a 100:5 lipid to DSSN+ molar ratio.[39] The mixture was incubated at 4 °C overnight for the DSSN+ reconstitution process. 100 µL of the mixture was added to a 96-well culture plate and emission intensity was read from 445 to 750 nm with a fixed excitation wavelength at 420 nm using a Spectra Max i3X instrument. Emission intensity was normalized from 0 to 1 and used for further analysis.

Supporting Information

Supporting Information is available from the Wiley Online Library or from the author.

Acknowledgements

This work was funded as a collaborative effort between the Kumar group at Penn State, Applied Biomimetic and the University of California, Santa Barbara, and was funded in part by Applied Biomimetic. Additional funding was provided by the National Science foundation through its GOALI program (Grant No. CBET – 1512099) and through another grant (CBET – 1552571). Work in the Bazan lab was funded through a grant from the U.S. Army Research Office (W911NF-09-0001). The authors would like to thank Dr. Mark Signs for his support on fermentations for membrane protein production and Michael J. Shreve and Prof. Rachel A. Brennan for providing access to their microplate reader (Spectra Max i3X).

Conflict of Interest

Applied Biomimetic contributed to this work and is a startup that is commercializing biomimetic membranes.

© 2017 WILEY-VCH Verlag GmbH & Co. KGaA, Weinheim

Keywords

amphiphilic block copolymers, biomimetic membranes, fluorescence correlation spectroscopy (FCS), hydrophobicity mismatch, membrane proteins

Received: March 8, 2017
Revised: May 7, 2017
Published online: June 16, 2017

[1] B. S. Vallée, P. Tauc, J.-C. Brochon, R. Maget-Dana, D. Lelièvre, M.-H. Metz-Boutigue, N. Bureaud, F. Schoentgen, *Eur. J. Biochem.* **2001**, *268*, 5831.
[2] S. Broselid, K. A. Berg, T. A. Chavera, R. Kahn, W. P. Clarke, B. Olde, L. M. F. Leeb-Lundberg, *J. Biol. Chem.* **2014**, *289*, 22117.
[3] M. D. Parker, E. J. Myers, J. R. Schelling, *Cell. Mol. Life Sci.* **2015**, *72*, 2061.
[4] C. H. Ko, S. C. Shen, T. J. F. Lee, Y. C. Chen, *Mol. Cancer Ther.* **2005**, *4*, 281.
[5] S. Belegrinou, J. Dorn, M. Kreiter, K. Kita-Tokarczyk, E.-K. Sinner, W. Meier, *Soft Matter* **2010**, *6*, 179.
[6] a) Y.-x. Shen, W. Si, M. Erbakan, K. Decker, R. De Zorzi, P. O. Saboe, Y. J. Kang, S. Majd, P. J. Butler, T. Walz, A. Aksimentiev, J.-l. Hou, M. Kumar, *Proc. Natl. Acad. Sci. USA* **2015**, *112*, 9810; b) X.-B. Hu, Z. Chen, G. Tang, J.-L. Hou, Z.-T. Li, *J. Am. Chem. Soc.* **2012**, *134*, 8384; c) B. Liu, X. Li, B. Li, B. Xu, Y. Zhao, *Nano Lett.* **2009**, *9*, 1386.
[7] J. Clarke, H.-C. Wu, L. Jayasinghe, A. Patel, S. Reid, H. Bayley, *Nat. Nanotechnol.* **2009**, *4*, 265.
[8] T. Karamitros, I. Harrison, R. Piorkowska, A. Katzourakis, G. Magiorkinis, J. L. Mbisa, *PLoS One* **2016**, *11*, e0157600.
[9] S. Mura, J. Nicolas, P. Couvreur, *Nat. Mater.* **2013**, *12*, 991.
[10] a) M. Kumar, M. Grzelakowski, J. Zilles, M. Clark, W. Meier, *Proc. Natl. Acad. Sci. USA* **2007**, *104*, 20719; b) P. S. Zhong, T. S. Chung, K. Jeyaseelan, A. Armugam, *J. Membr. Sci.* **2012**, *407*, 27.
[11] M. Erbakan, Y.-X. Shen, M. Grzelakowski, P. J. Butler, M. Kumar, W. R. Curtis, *PLoS One* **2014**, *9*, e86830.
[12] O. S. Andersen, R. E. Koeppe, *Annu. Rev. Biophys. Biomol. Struct.* **2007**, *36*, 107.
[13] M. P. E. van Heeswijk, C. H. van Os, *J. Membr. Biol.* **1986**, *92*, 183.
[14] D. G. Knyazev, A. Lents, E. Krause, N. Ollinger, C. Siligan, D. Papinski, L. Winter, A. Horner, P. Pohl, *J. Biol. Chem.* **2013**, *288*, 17941.
[15] H. Wang, T. S. Chung, Y. W. Tong, K. Jeyaseelan, A. Armugam, Z. Chen, M. Hong, W. Meier, *Small* **2012**, *8*, 1185.
[16] W. Y. Xie, F. He, B. F. Wang, T. S. Chung, K. Jeyaseelan, A. Armugam, Y. W. Tong, *J. Mater. Chem. A* **2013**, *1*, 7592.
[17] A. Laganowsky, E. Reading, T. M. Allison, M. B. Ulmschneider, M. T. Degiacomi, A. J. Baldwin, C. V. Robinson, *Nature* **2014**, *510*, 172.
[18] a) M. J. Borgnia, D. Kozono, G. Calamita, P. C. Maloney, P. Agre, *J. Mol. Biol.* **1999**, *291*, 1169; b) D. Gessmann, Y. H. Chung, E. J. Danoff, A. M. Plummer, C. W. Sandlin, N. R. Zaccai, K. G. Fleming, *Proc. Natl. Acad. Sci. USA* **2014**, *111*, 5878.
[19] L. E. Garner, J. Park, S. M. Dyar, A. Chworos, J. J. Sumner, G. C. Bazan, *J. Am. Chem. Soc.* **2010**, *132*, 10042.
[20] J. R. Lakowicz, *Principles of Fluorescence Spectroscopy*, Springer, New York, **2013**.
[21] P. H. H. Duong, T.-S. Chung, K. Jeyaseelan, A. Armugam, Z. Chen, J. Yang, M. Hong, *J. Membr. Sci.* **2012**, *409–410*, 34.
[22] a) Y.-x. Shen, P. O. Saboe, I. T. Sines, M. Erbakan, M. Kumar, *J. Membr. Sci.* **2014**, *454*, 359; b) M. Kumar, M. M. Payne, S. K. Poust, J. L. Zilles, in *Biomimetic Membranes for Sensor and Separation Applications* (Ed: C. Hélix-Nielsen), Springer, Dordrecht, The Netherlands **2012**, p. 43.
[23] M. Erbakan, B. S. Curtis, B. T. Nixon, M. Kumar, W. R. Curtis, *Protein Expression Purif.* **2015**, *115*, 109.
[24] a) T. Hoomann, N. Jahnke, A. Horner, S. Keller, P. Pohl, *Proc. Natl. Acad. Sci. USA* **2013**, *110*, 10842; b) M. Erbakan, Y.-x. Shen, P. J. Butler, M. Kumar, W. R. Curtis, *PLoS One* **2014**, *9*, e86830.
[25] a) J. Habel, M. Hansen, S. Kynde, N. Larsen, S. R. Midtgaard, G. V. Jensen, J. Bomholt, A. Ogbonna, K. Almdal, A. Schulz, C. Hélix-Nielsen, *Membranes* **2015**, *5*, 307; b) A. González-Pérez, K. B. Stibius, T. Vissing, C. H. Nielsen, O. G. Mouritsen, *Langmuir* **2009**, *25*, 10447; c) H. L. Wang, T.-S. Chung, Y. W. Tong, K. Jeyaseelan, A. Armugam, H. H. P. Duong, F. Fu, H. Seah, J. Yang, M. Hong, *J. Membr. Sci.* **2013**, *434*, 130.
[26] W. Meier, C. Nardin, M. Winterhalter, *Angew. Chem.* **2000**, *39*, 4599.
[27] a) X. Li, R. Wang, F. Wicaksana, C. Tang, J. Torres, A. G. Fane, *J. Membr. Sci.* **2014**, *450*, 181; b) A. Laganowsky, E. Reading, T. M. Allison, M. B. Ulmschneider, M. T. Degiacomi, A. J. Baldwin, C. V. Robinson, *Nature* **2014**, *510*, 172.
[28] A. Chabanel, M. Flamm, K. L. Sung, M. M. Lee, D. Schachter, S. Chien, *Biophys. J.* **1983**, *44*, 171.
[29] a) J. G. Bernstein, E. S. Boyden, *Trends Cognit. Sci.* **2011**, *15*, 592; b) F. Zhang, J. Vierock, O. Yizhar, L. E. Fenno, S. Tsunoda, A. Kianianmomeni, M. Prigge, A. Berndt, J. Cushman, J. Polle, J. Magnuson, P. Hegemann, K. Deisseroth, *Cell* **2011**, *147*, 1446.
[30] a) F. Itel, A. Najer, C. G. Palivan, W. Meier, *Nano Lett.* **2015**, *15*, 3871; b) G. Srinivas, D. E. Discher, M. L. Klein, *Nano Lett.* **2005**, *5*, 2343; c) Z. Bai, B. Zhao, T. P. Lodge, *J. Phys. Chem. B* **2012**, *116*, 8282.
[31] H. Bermudez, A. K. Brannan, D. A. Hammer, F. S. Bates, D. E. Discher, *Macromolecules* **2002**, *35*, 8203.
[32] F. Itel, M. Chami, A. Najer, S. Lörcher, D. Wu, I. A. Dinu, W. Meier, *Macromolecules* **2014**, *47*, 7588.
[33] a) P. J. Flory, *J. Chem. Phys.* **1942**, *10*, 51; b) M. L. Huggins, *J. Chem. Phys.* **1941**, *9*, 440.
[34] a) M. Kumar, J. E. O. Habel, Y.-x. Shen, W. P. Meier, T. Walz, *J. Am. Chem. Soc.* **2012**, *134*, 18631; b) S. S. Klara, P. O. Saboe, I. T. Sines, M. Babaei, P.-L. Chiu, R. DeZorzi, K. Dayal, T. Walz, M. Kumar, M. S. Mauter, *J. Am. Chem. Soc.* **2016**, *138*, 28.
[35] A. J. Heron, J. R. Thompson, A. E. Mason, M. I. Wallace, *J. Am. Chem. Soc.* **2007**, *129*, 16042.
[36] a) H. Herberhold, S. Marchal, R. Lange, C. H. Scheyhing, R. F. Vogel, R. Winter, *J. Mol. Biol.* **2003**, *330*, 1153; b) R. S. Kaplan, P. L. Pedersen, *Anal. Biochem.* **1985**, *150*, 97; c) B. C. McIlwain, R. J. Vandenberg, R. M. Ryan, *J. Biol. Chem.* **2015**, *290*, 9780.
[37] P. E. Milhiet, M. C. Giocondi, O. Baghdadi, F. Ronzon, C. Le Grimellec, B. Roux, *Single Mol.* **2002**, *3*, 135.
[38] R. R. Gullapalli, T. Tabouillot, R. Mathura, J. H. Dangaria, P. J. Butler, *J. Biomed. Opt.* **2007**, *12*, 014012.
[39] P. O. Saboe, E. Conte, S. Chan, H. Feroz, B. Ferlez, M. Farell, M. F. Poyton, I. T. Sines, H. Yan, G. C. Bazan, J. Golbeck, M. Kumar, *J. Mater. Chem. A* **2016**, *4*, 15457.

 © 2017 WILEY-VCH Verlag GmbH & Co. KGaA, Weinheim